https://ntrs.nasa.gov/search.jsp?R=19870017542 2020-03-20T09:29:17+00:00Z

NAG1-392

SEMIANNUAL REPORT

MODELING OF TRANSIENT HEAT PIPE OPERATION

By

Gene T. Colwell
James G. Hartley

Period Covered
February 19, 1986 through August 18, 1986

Submitted to

National Aeronautics and Space Administration
Langley Research Center
Hampton, Virginia 23665

NASA Technical Officer
Charles J. Camarda
Mail Stop 396

Under

NASA GRANT NAG-1-392

November 1, 1986

GEORGIA INSTITUTE OF TECHNOLOGY
A UNIT OF THE UNIVERSITY SYSTEM OF GEORGIA
SCHOOL OF MECHANICAL ENGINEERING
ATLANTA, GEORGIA 30332

1986

NASA GRANT NAG-1-392

MODELING OF TRANSIENT HEAT PIPE OPERATION

BY

Gene T. Colwell and James G. Hartley
School of Mechanical Engineering
Atlanta, Georgia 30332

Submitted to

National Aeronautics and Space Administration
Langley Research Center
Hampton, Virginia 23665

NASA Technical Officer
Charles J. Camarda
Mail Stop 396

Period Covered
February 19, 1986 through August 18, 1986

November 1, 1986

TABLE OF CONTENTS

INTRODUCTION

This report summarizes progress made on NASA Grant NAG-1-392 during the period February 19, 1986 through August 18, 1986. The goal of the project is to develop mathematical models and associated solution procedures which can be used to design heat pipe cooled structures for use on hypersonic vehicles. The models should also have the capability to predict off-design performance for a variety of operating conditions. It is expected that the resulting models can be used to predict startup behavior of liquid metal heat pipes to be used in reentry vehicles, hypersonic aircraft and space nuclear reactors.

Previous reports in this series (February 1985, September 1985 and June 1986) have covered the development of governing differential equations which can be used to predict startup behavior of initially frozen liquid metal heat pipes. The June 1986 report covered the development of finite element based numerical equations for the outer shell and the combination capillary structure and working fluid. One and two dimension transient solutions were presented.

The current report covers mathematical models and sample solutions for the vapor region. The heat pipe considered is rectangular, the working vapor is sodium and the initial temperature is sufficiently low so that the capillary structure is filled with solid sodium.

ANALYSIS OF VAPOR FLOW IN HEAT PIPES

Analysis of the hydrodynamics of vapor flow in heat pipes with metallic working fluids indicates considerable difficulties at low vapor pressure due to the extremely small vapor densities. Even for

relatively small heat transfer rates, the vapor velocity in the axial direction can be very large and accelerated towards sonic velocity by friction at the interface. Additional heat input causes choking at the condenser inlet. Such behavior makes it necessary to include vapor compressibility and viscous action in mathematical models. Vapor pressure drop due to friction can not be recovered completely in the condensation section. Thus, the temperature distributions along the length of the heat pipe are not isothermal and thermal resistance in the vapor region is significant. Therefore, studies of the distributions of temperature, pressure, and velocity in the vapor passage along the length of a heat pipe are essential for an evaluation of the maximum heat transfer rates and prediction of correct heat pipe performance.

A summary of the literature on hydrodynamic processes in vapor flow of cylindrical heat pipes made by Tien [1] and Ivanovskii et. al. [2] indicates that no completely detailed investigation has been presented thus far. Moreover, experimental measurements of pressure and velocity for metallic working fluids have not been reported.

In the present paper, an analysis of the steady, compressible, one-dimensional, laminar flow of sodium vapor is presented for the case of a flat plate-type heat pipe with asymmetrical boundary conditions. In addition, shear stress at the liquid-vapor interface, variations of vapor quality, and momentum and energy factors are considered. A similarity solution for a semiporous channel is used to provide the velocity profile at cross sections.

1. Similarity Solution for Semiporous Channel

Governing Differential Equations

A sketch of the geometry for a semiporous channel is given in Figure 1. The following assumptions are made : that the fluid flow is incompressible and laminar, and that the properties of the fluid are constant. The width of the channel is assumed much greater than the height. Therefore, two-dimensional flow is considered. Fully developed flow is assumed in the channels. A constant injection or suction velocity is used. With these assumptions, the Navier-Stokes equations for two-dimensional steady state incompressible laminar flow are written as

$$u \frac{\partial u}{\partial z} + v^* \frac{\partial u}{\partial y} = - \frac{1}{\rho} \frac{\partial p}{\partial z} + \nu \left(\frac{\partial^2 u}{\partial z^2} + \frac{\partial^2 u}{\partial y^2} \right) \tag{1}$$

$$u \frac{\partial v^*}{\partial z} + v^* \frac{\partial v^*}{\partial y} = - \frac{1}{\rho} \frac{\partial p}{\partial y} + \nu \left(\frac{\partial^2 v^*}{\partial z^2} + \frac{\partial^2 v^*}{\partial y^2} \right) \tag{2}$$

and the continuity equation is

$$\frac{\partial u}{\partial z} + \frac{\partial v^*}{\partial y} = 0 \tag{3}$$

The boundary conditions used on the channel surfaces are

$u = 0$, and $v^* = 0$ at $y = 0$ (solid wall)

$u = 0$, and $v^* = v_o^*$ at $y = D$ (porous wall)

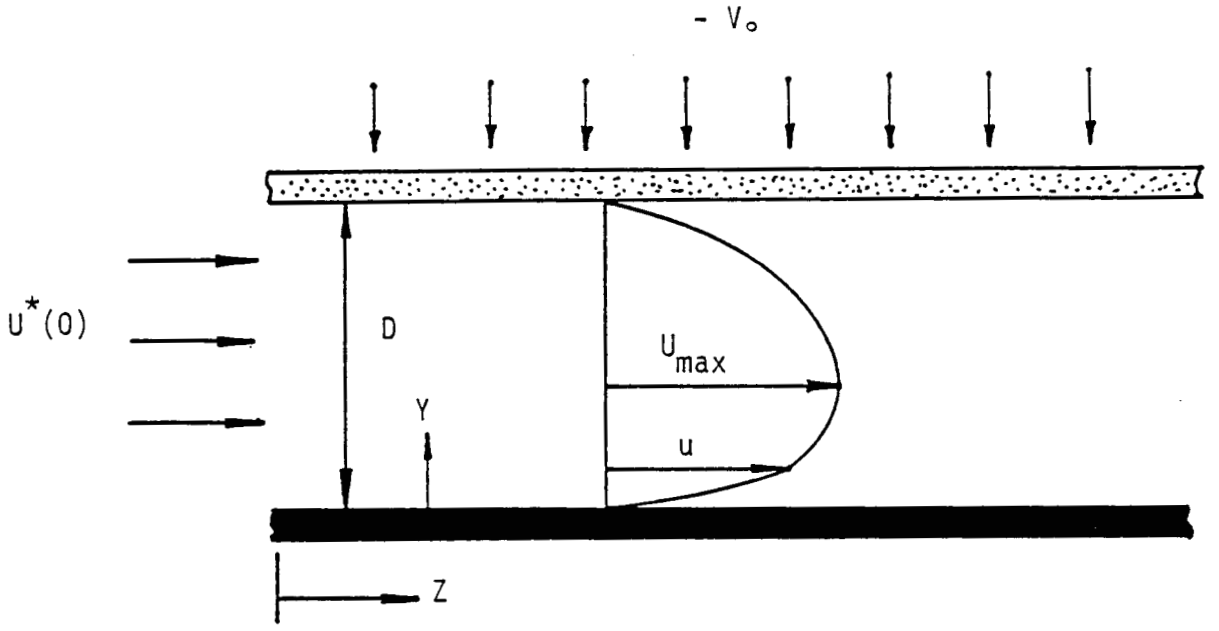

- V_o : Injection, depicted.

V_o : Suction.

Figure 1. Schematic diagram of a semiporous channel.

Similarity Transformations

The governing equations can be transformed into total differential equations by the use of a dimensionless length coordinate, λ, and a dimensionless function, f, which automatically satisfies the continuity equation. The new variables are defined as

$$\lambda = \frac{y}{D} \tag{6}$$

$$f(\lambda) = \frac{\psi}{Dv} \tag{7}$$

where $V(z) = U^*(0) - \frac{v_o^* z}{D}$

and $U^*(0)$ is the average velocity at $z = 0$. Then, the local velocity can be expressed by the new variables as follows

$$u = \frac{1}{D} \frac{\partial \psi}{\partial y} = Vf' \tag{8}$$

$$v^* = - \frac{\partial \psi}{\partial z} = v_o^* f \tag{9}$$

Use of equations(1), (2), and (6) to (9) gives

$$- \frac{1}{\rho} \frac{\partial p}{\partial z} = V\left[\frac{v_o^*}{D} (ff'' - (f')^2 - \frac{\nu}{D^2} f''') \right] \tag{10}$$

$$- \frac{1}{\rho} \frac{\partial p}{\partial \lambda} = v_o^* \left[v_o^* ff' - \frac{\nu}{D} f'' \right] \tag{11}$$

Since the right side of equation (11) is a function of λ only, differentiating with respect to λ yields

$$\frac{\partial^2 p}{\partial z \partial \lambda} = 0 \qquad (12)$$

On taking the derivative with respect to λ, using equation (12), and integrating, equation (10) becomes

$$Re_o \left[(f')^2 - ff''\right] + f''' = - A \qquad (13)$$

where $Re_o = \frac{v_o * D}{\nu}$ and $A = - \frac{D^2}{\nu \rho} \frac{\partial p}{\partial x}$

The transformed boundary conditions are written as

$f' = f = 0$ at $\lambda = 0$ (solid wall) (14)

$f' = 0,\ f = 1$ at $\lambda = 1$ (porous wall) (15)

Solution of Equation

The differential equation(13) together with the associated boundary conditions constitute a nonlinear boundary value problem with the parameter Re_o. Since the governing equations are no longer partial differential equations, they can be solved numerically by the Runge-Kutta integration method. However, the number of boundary conditions is not enough to solve the equation(13). Therefore, for each specified Re_o, the value of A and f"(0) are guessed to solve the system

of the first order differential equations. Then, at $\lambda = 1$(porous wall), the calculated values of f' and f are compared with the given boundary conditions. When both values are not acceptable, other values are used until the tolerance is satisfied. When wall Reynolds numbers for suction are greater than 13, separation occurs on the solid wall. Similarity solutions are valid for wall Reynolds numbers up to 13. Hence, the equation is solved for wall Reynolds numbers ranging from - 30 to 13.

A comparison of the present results with those found in the literature [3,4], which used the perturbation method for small Reynolds numbers, and a different numerical scheme, verifies the accuracy of the numerical solution.

The velocity profiles for the suction and injection sections are shown in Figures 2 and 3. Asymmetric boundary conditions means that the velocity profiles are asymmetric. For injection, $Re_o < 0$, the location of the maximum velocity shifts from the center of channels to the solid wall. Thus, injection increases friction at the solid wall, and decreases friction at the porous wall. As wall Reynolds numbers increase, the degree of shifting is large. However, the general shape is changed little. For suction, $Re_o > 0$, the location of the peak velocity shifts toward the porous wall. Hence, suction increases friction at the porous wall and decreases friction at the solid wall. Unlike injection, separation appears around a wall Reynolds number of 13. The velocity profiles change considerably with wall Reynolds numbers. In general, friction for the semiporous channel is larger than that for the impermeable channel.

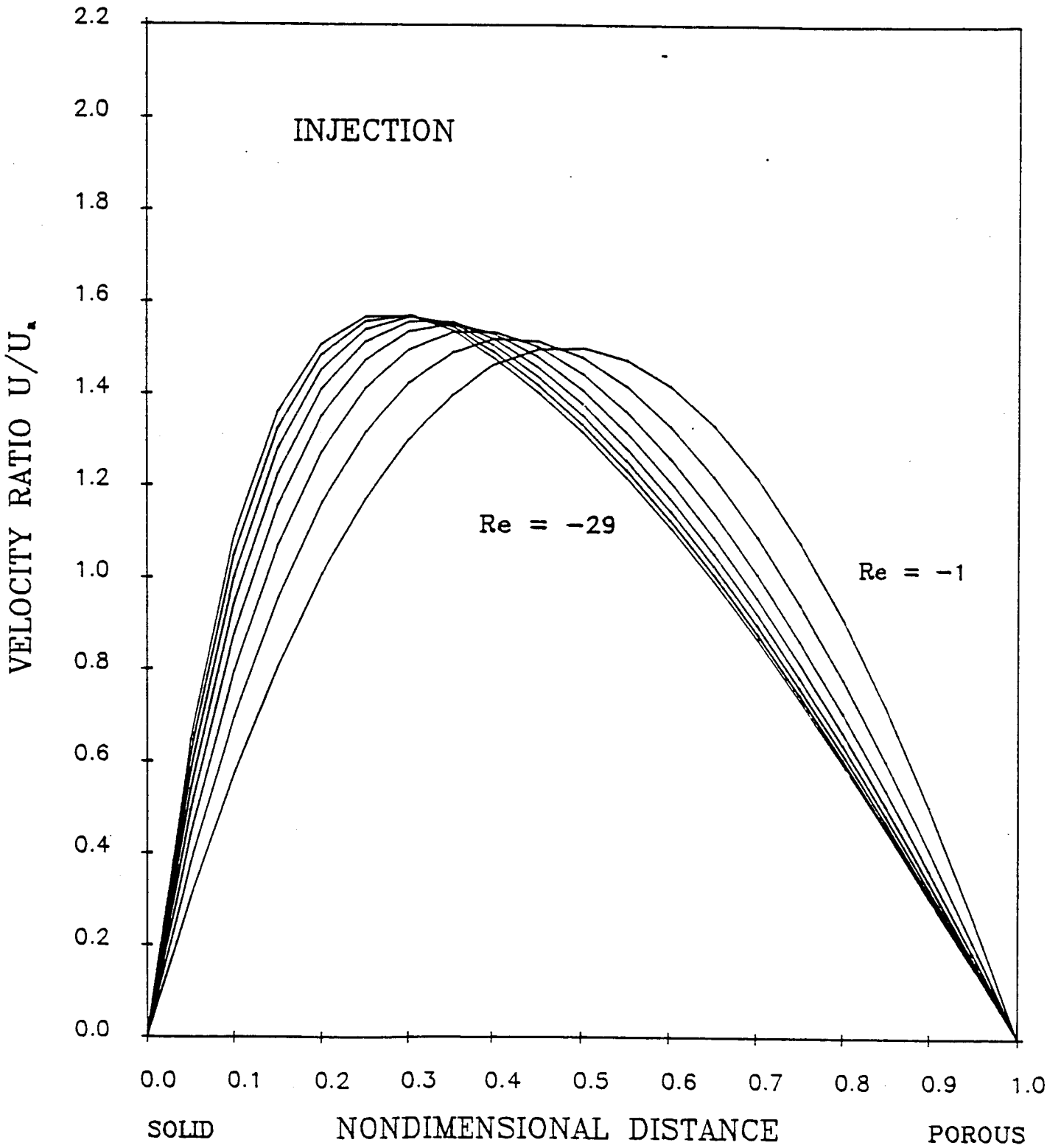

Figure 2. Velocity profiles with wall injection in a semiporous channel.

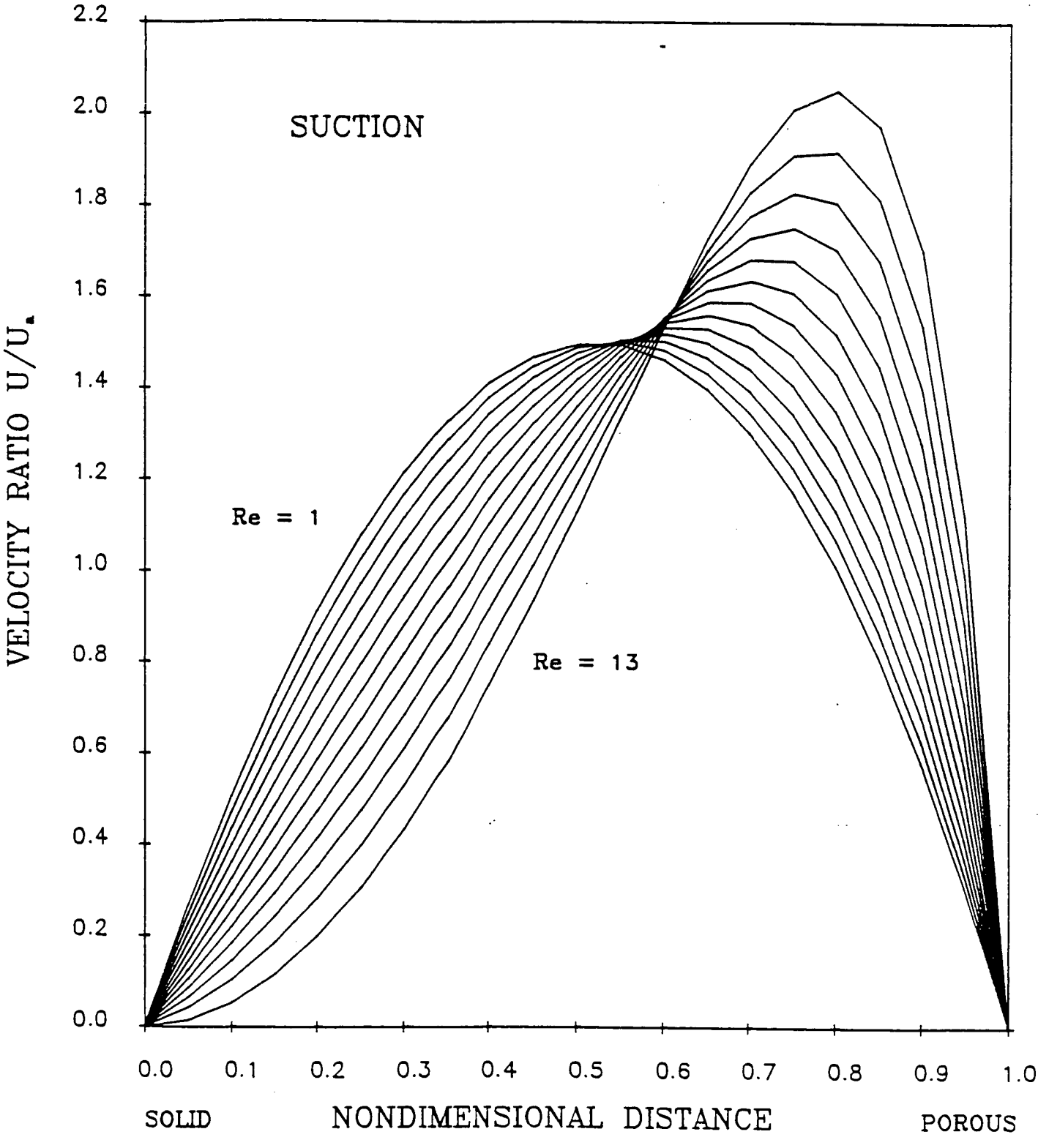

Figure 3. Velocity profiles with wall suction in a semiporous channel.

2. Compressible Vapor Flow Analysis

Steady, compressible, one-dimensional laminar flow in a heat pipe is considered. The heat pipe under study is shown schematically in Figure 4. For purposes of formulating the mass, momentum, and energy equations in one-dimensional form, the velocity is taken to be the average velocity, which is approximated by the velocity distributions based on the similarity solution of semiporous channels. Shear stress at the interface and the momentum and energy factors are similarly calculated and shown in Figure 5. The vapor is evaporated at the liquid-vapor interface with mass injection rate, $\dot{m}_o$, per unit area. It is assumed that this vapor flows inward with a normal component of velocity only, and joins the axial flowing stream.

Principle Governing Equations

The principles of conservation of mass, momentum, and energy in the axial direction, and the previously mentioned assumption, yield

$$D \frac{d}{dz} (\rho V) = \dot{m}_o \tag{16}$$

$$\frac{dP}{dz} + \frac{d}{dz} (\alpha \rho V^2) = - \frac{F \rho V^2}{8D} \tag{17}$$

$$D \frac{d}{dz} \left[\rho V \left(h + \frac{\beta V^2}{2}\right)\right] = \dot{m}_o \left(h_o + \frac{v_o^{*2}}{2}\right) \tag{18}$$

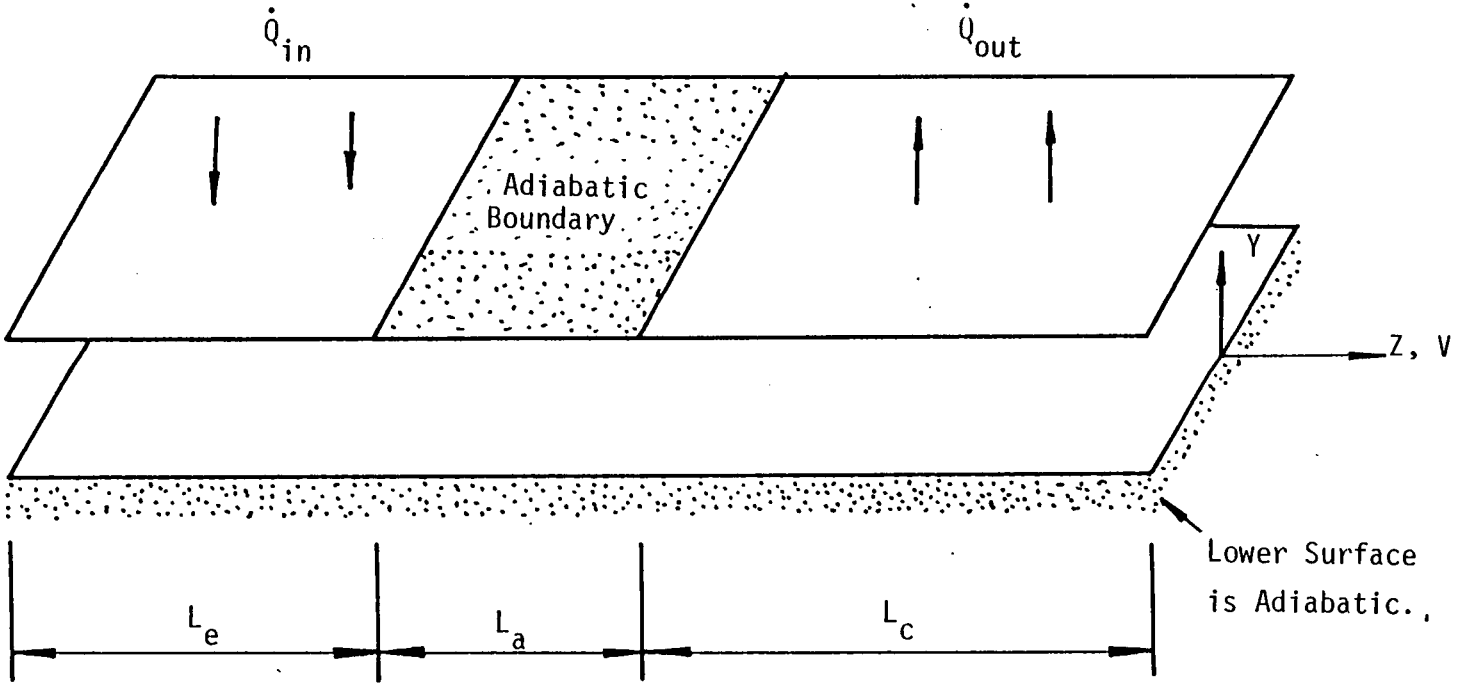

Figure 4. Heat pipe vapor region.

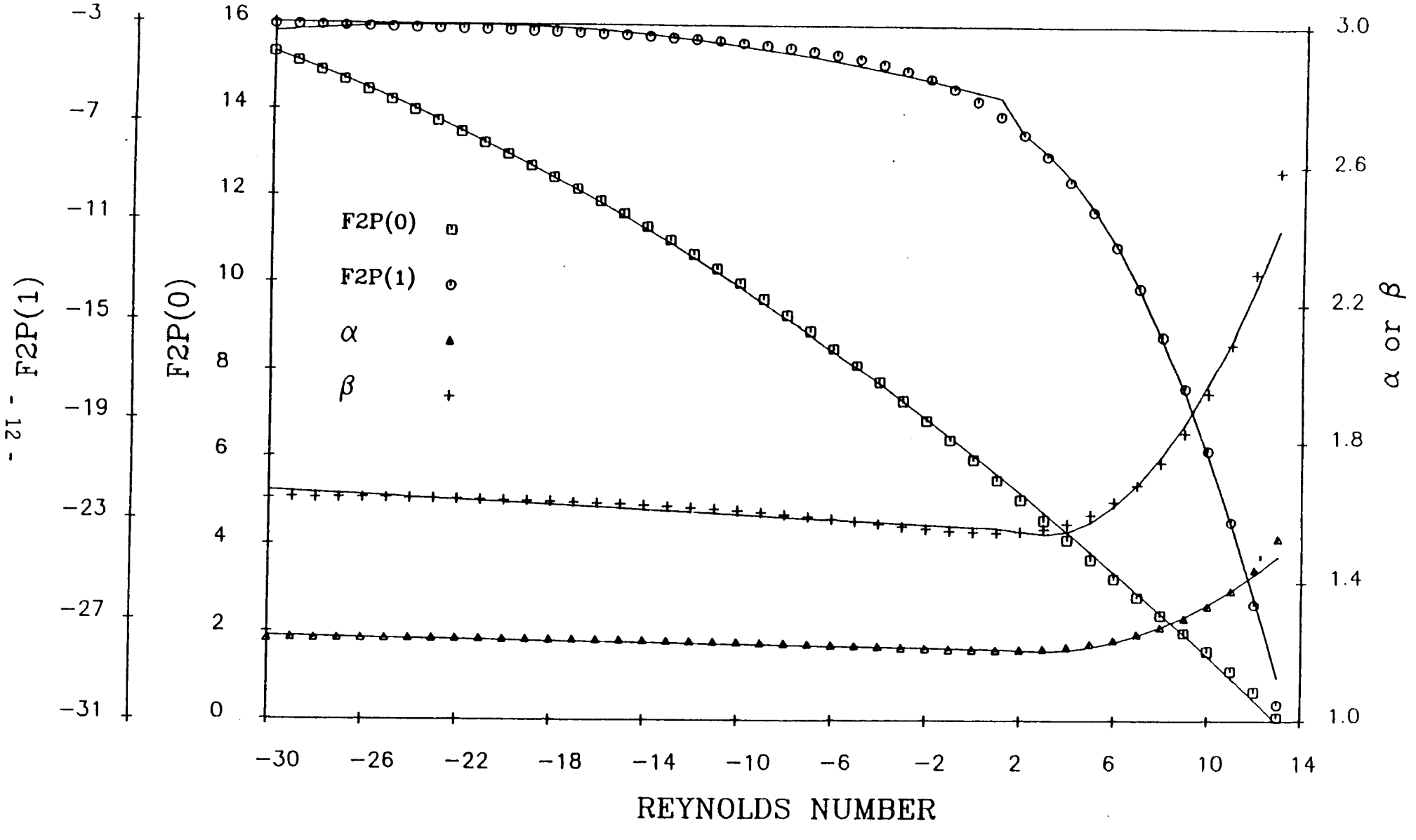

Figure 5. Variations of momentum and energy factors, and friction with wall Reynolds numbers.

where D is the thickness of the heat pipe and h is the vapor enthalpy. The friction factor, F, of the surfaces is written as

$$F = \frac{8\tau_v}{\rho V^2} \tag{19}$$

The momentum and energy factors, α and β, respectively, are expressed as

$$\alpha = \frac{1}{DV^2} \int_o^D u^2 \, dy \tag{20}$$

$$\beta = \frac{1}{DV^3} \int_o^D u^3 \, dy \tag{21}$$

The normal velocity of the vapor at the interface is expressed in terms of the heat flux and latent heat of vaporization as follows

$$v_o^* = \frac{Q}{h_{fg} \cdot \rho_o \cdot A_o} \tag{22}$$

The fluid in the vapor passage of the heat pipe is assumed to be a mixture of liquid and monotonic vapor. Thus, the quality of the vapor is considered. The specific volume v and the enthalpy h are expressed as

$$v = v_f + x \cdot (v_g - v_f) \tag{23}$$

$$h = h_f + x \cdot h_{fg} \tag{24}$$

The specific volume of the saturated vapor can be approximated by

$$v_g = \frac{RT}{P} \tag{25}$$

Also, the temperature and pressure are related by the Clausius-Clapyron equation:

$$\frac{dP}{P} = \frac{h_{fg}}{R} \cdot \frac{dT}{T^2} \tag{26}$$

where h_{fg} is the enthalpy of saturated liquid, v_f and v_g are the specific volume of saturated liquid and vapor, respectively, and X is the vapor quality.

Formulations of Differential Equations

Bankston et. al.[5] showed that variation of the momentum and energy factors with axial distance and radial Reynolds numbers is very small except near the end of the heat pipe. Also, Figure 5 shows both α and β are nearly independent of the radial Reynolds numbers except near separation. These results are taken from the calculations for the similarity solution of the semiporous channels. Therefore, it is assumed that the derivative of α and β with respect to axial distance is equal to zero. In addition, assuming v_f and h_{fg} are constant quantities, and combining equations (16) thru (26) yields the axial gradients for the density, quality, velocity, pressure, and temperature.

Density

The differentiation of equation (25) with respect to z gives

$$\frac{dv_g}{dZ} = -\frac{v_g}{P}\frac{dP}{dZ} + \frac{v_g}{T}\frac{dT}{dZ} \tag{27}$$

Substitution of equation(26) into the equation above yields

$$\frac{dv_g}{dZ} = \frac{v_g}{P}\left[\frac{RT}{h_{fg}} - 1\right]\frac{dP}{dZ} \tag{28}$$

The derivative of specific volume in the z-direction is written as

$$\frac{dv}{dZ} = \frac{dv_f}{dZ} + (v_g - v_f)\frac{dx}{dz} + x \bullet \left[\frac{dv_g}{dZ} - \frac{dv_f}{dZ}\right] \tag{29}$$

With the prescribed assumption for v_f, substitution of equation (28) into (29) obtains

$$\frac{dv}{dZ} = (v_g - v_g)\frac{dx}{dZ} + \frac{v_g x}{P}\left[\frac{RT}{h_{fg}} - 1\right]\frac{dP}{dZ} \tag{30}$$

Also, the derivative of specific volume and density are related as follows

$$\frac{d\varrho}{dZ} = -\frac{1}{v^2}\frac{dv}{dZ} \tag{31}$$

From equations (30) and (31), the expression of density in differential form can be written as

$$\frac{d\rho}{dZ} = -\frac{1}{v^2}\left[\left(v_g - v_f\right)\frac{dx}{dZ} + \frac{v_g x}{P}\left(\frac{RT}{h_{fg}} - 1\right)\frac{dP}{dZ}\right] \tag{32}$$

Quality

From equation(9), the quality gradient is expressed as

$$\frac{dx}{dZ} = \frac{v}{(v_g - v_f)}\left[\frac{dV}{dZ} + \frac{v_g x}{P}\left(1 - \frac{RT}{h_{fg}}\right)\frac{dP}{dZ}\right] \tag{33}$$

Substitution of equation (31), equations of the conservation of mass, and momentum into equation (33) yields

$$\frac{dx}{dZ} = \frac{v^2}{(v_g - v_f)V^2}\left\{\left[-\frac{1}{\alpha} + \frac{V^2 x}{P} \cdot \frac{v_g}{v^2}\left(1 - \frac{RT}{h_{fg}}\right)\right]\frac{dP}{dz} - \frac{FV^2}{8Dv\alpha}\right\} \tag{34}$$

$$- \frac{v^2}{(v_g - v_f)} \cdot \frac{2\dot{m}_o}{DV}$$

Velocity

The equation of the conservation of mass can be expressed as follows

$$\frac{dV}{dZ} = \frac{v\dot{m}_o}{D} + \frac{V}{v}\frac{dV}{dZ} \tag{35}$$

Substitution of equation(30) into the expression above gives

$$\frac{dV}{dZ} = \frac{\dot{vm}_o}{D} + \frac{V(v_g - v_f)}{v}\frac{dx}{dz} + \frac{Vx}{P}\frac{v_g}{v}\left[\frac{R\bar{T}}{h_{fg}} - 1\right]\frac{dP}{dZ} \qquad (36)$$

Pressure

With the previously mentioned assumptions, substitution of the energy equation (18) into the momentum equation yields

$$\frac{dP}{dZ} - \frac{\alpha\rho}{\beta}\frac{dh}{dZ} - \frac{\dot{\alpha m}_o}{\beta VD}\left[h - h_o - \frac{\beta V^2}{2} - \frac{v_o{}^{*2}}{2}\right] = -\frac{F\rho V^2}{8D} \qquad (37)$$

In order to obtain an expression for the derivative of the vapor enthalpy, differentiation of equation (24) is taken with respect to Z, and equation (26) is substituted:

$$\frac{dh}{dZ} = h_{fg}\frac{dx}{dZ} + \frac{C_{pf}R}{h_{fg}} \cdot \frac{T^2}{P}\frac{dP}{dZ} \qquad (38)$$

After the expressions for the derivative of the enthalpy and quality are substituted into equation (36), the pressure gradient can be expressed as follows

$$\frac{dP}{dZ} = \frac{-\frac{\dot{\alpha m}_o}{\beta vD}\left[2h_{fg} + \frac{v_g - v_f}{v}\left[h_o - h + \frac{\beta V^2}{2} + \frac{v_o{}^{*2}}{2}\right]\right] - \frac{1}{\beta}\frac{h_{fg}}{v}\frac{F}{8D} - \frac{v_g - v_f}{v^2}\cdot\frac{FV^2}{8D}}{\frac{v_g - v_f}{v} + \frac{1}{\beta}\frac{h_{fg}}{V^2} - \frac{\alpha}{\beta}\cdot\frac{h_{fg}x}{P}\cdot\frac{v_g}{v^2}\left[1 - \frac{RT}{h_{fg}}\right] - \frac{\alpha}{\beta}\cdot\frac{(v_g - v_f)}{v^2}\cdot\frac{C_{pf}R}{h_{fg}}\cdot\frac{T^2}{P}} \qquad (39)$$

Temperature

The temperature gradient is derived from the Clausius-Clapyron equation as follows

$$\frac{dT}{dZ} = \frac{RT^2}{h_{fg}P} \cdot \frac{dP}{dZ} \tag{40}$$

Description of Numerical Scheme

The five dependent variables, i.e. density, quality, velocity, pressure, and temperature, are coupled by the differential equations (32), (34), (36), (39), and (40) which are first order, nonlinear, and ordinary differential equations. A computer code has been written to solve these equations numerically and simultaneously using the Runge-Kutta integral method, which needs only proper boundary conditions for the first step of integration.

Since the velocity term appears at the denominator of equation (39), the physical boundary condition for velocity can not be used directly. To avoid this problem, proper boundary conditions at the upstream end of the evaporator are determined to initiate all calculations as follows: a new boundary condition for the velocity is determined at a short distance away from the beginning of the evaporator, assuming incompressible and saturated vapor flow at the temperature corresponding to the heat pipe operating temperature. Also, the saturation pressure is used for the pressure. Since the velocity is small at this point close to the upstream end of the evaporator, boundary conditions determined this way are realistic. The differential equations are solved by using these boundary conditions.

Results and Discussion

To investigate various effects, two types of heat pipes with sodium as the working fluid were selected for the analysis. One has an adiabatic section, the other does not. The dimensions of the heat pipes are shown in Table 1. Also, two different operating temperatures are chosen such that, for low operating temperatures, the pressure drop along the heat pipe is relatively large at the same heat flux. For each operating temperature, several cases of heat pipe operation with various heat fluxes are considered. Since the similarity solutions used are valid only while wall Reynolds numbers are less than 14, the maximum heat flux on the condenser is chosen to satisfy this condition.

Dimension	773°K	808°K
L_e (cm)	8.0	20.0
L_a	0.0	10.0
L_c	22.0	30.0
D	1.33	1.35
W	1.33	1.72
A_o (cm^2)	10.64	34.4

Table 1. Primary Information on Sodium Heat Pipes.

Figure 6 shows axial variations of vapor temperature, pressure, velocity, and density which are obtained from equations (32), (34), (36), (39), and (40). The operating temperature of 773 K, and the uniformly distributed heat transfer rate of 200 watts are used. Momentum equation (17) implies that the variation of pressure in the axial direction depends on the relation between the contributions from inertia and friction. Thus, the pressure of the vapor in the evaporator falls sharply along the vapor passage due to friction and the acceleration of the flow due to the injection of mass. The corresponding temperature also drops sharply about 5.5 K. Since the density of sodium vapor is relatively low at the low operating temperature, the velocity is correspondingly large to transfer the required mass. The results show the maximum Mach number reaches 0.3 at the exit of the evaporator.

In the condenser, the extraction of mass leads to a deceleration of the vapor flow so that pressure increases, while friction reduces the pressure. Therefore, the pressure can not recover completely due to friction loss. Even though temperature recovery is achieved in the condenser, the temperature at the end of the condenser is about 4.2 K less than that at the beginning of the evaporator. Therefore, the vapor passage in the heat pipe is not isothermal.

Figures 7, 8, and 9 show variations of temperature, pressure, and Mach number, respectively, corresponding to five different heat fluxes. At the same operating temperature of 773 K, a larger heat input leads to greater pressure and temperature drops, and to a higher Mach number. When

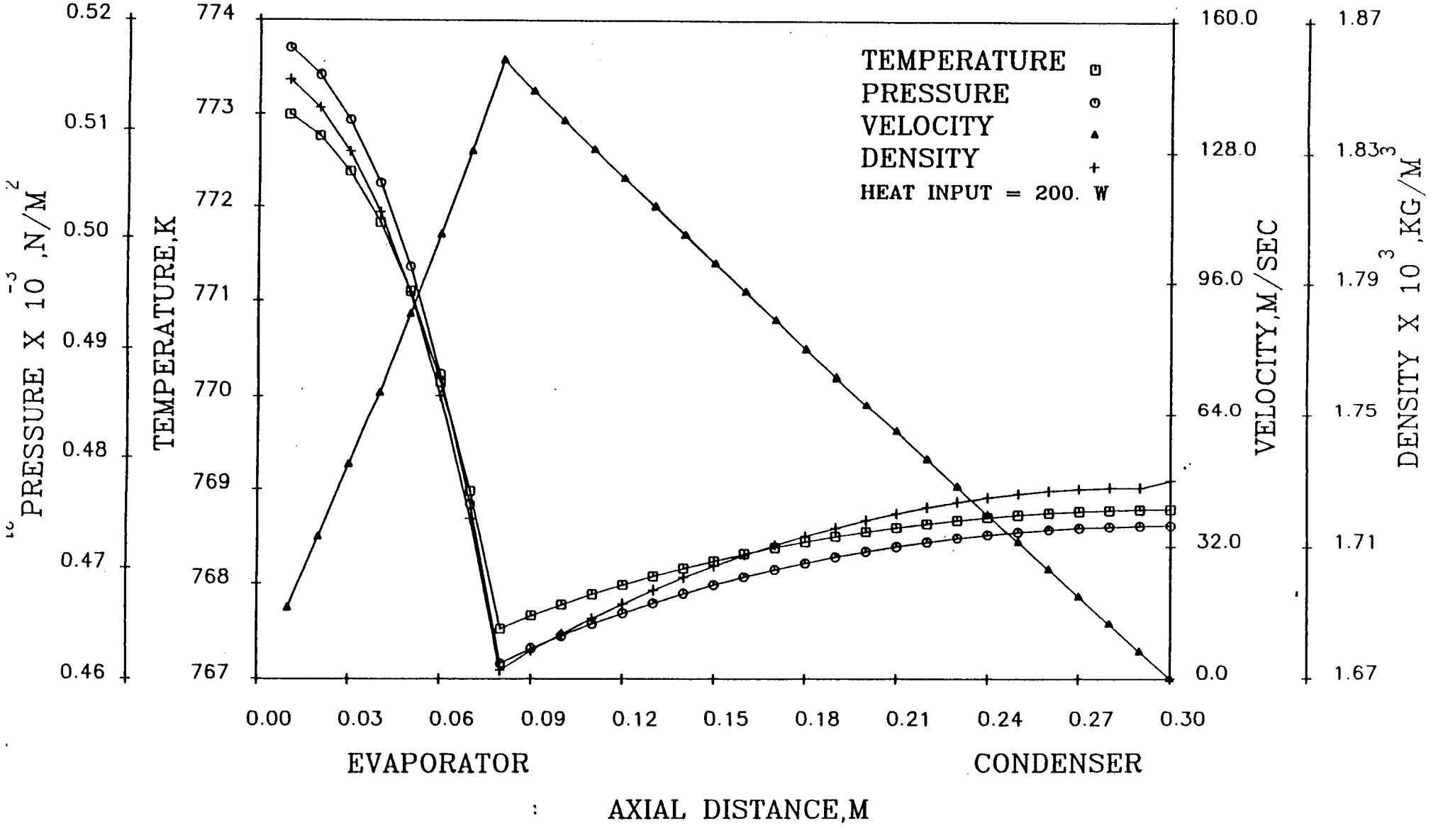

Figure 6. Axial variations of vapor temperature, pressure, velocity, and density at operating temperature of 773 k.

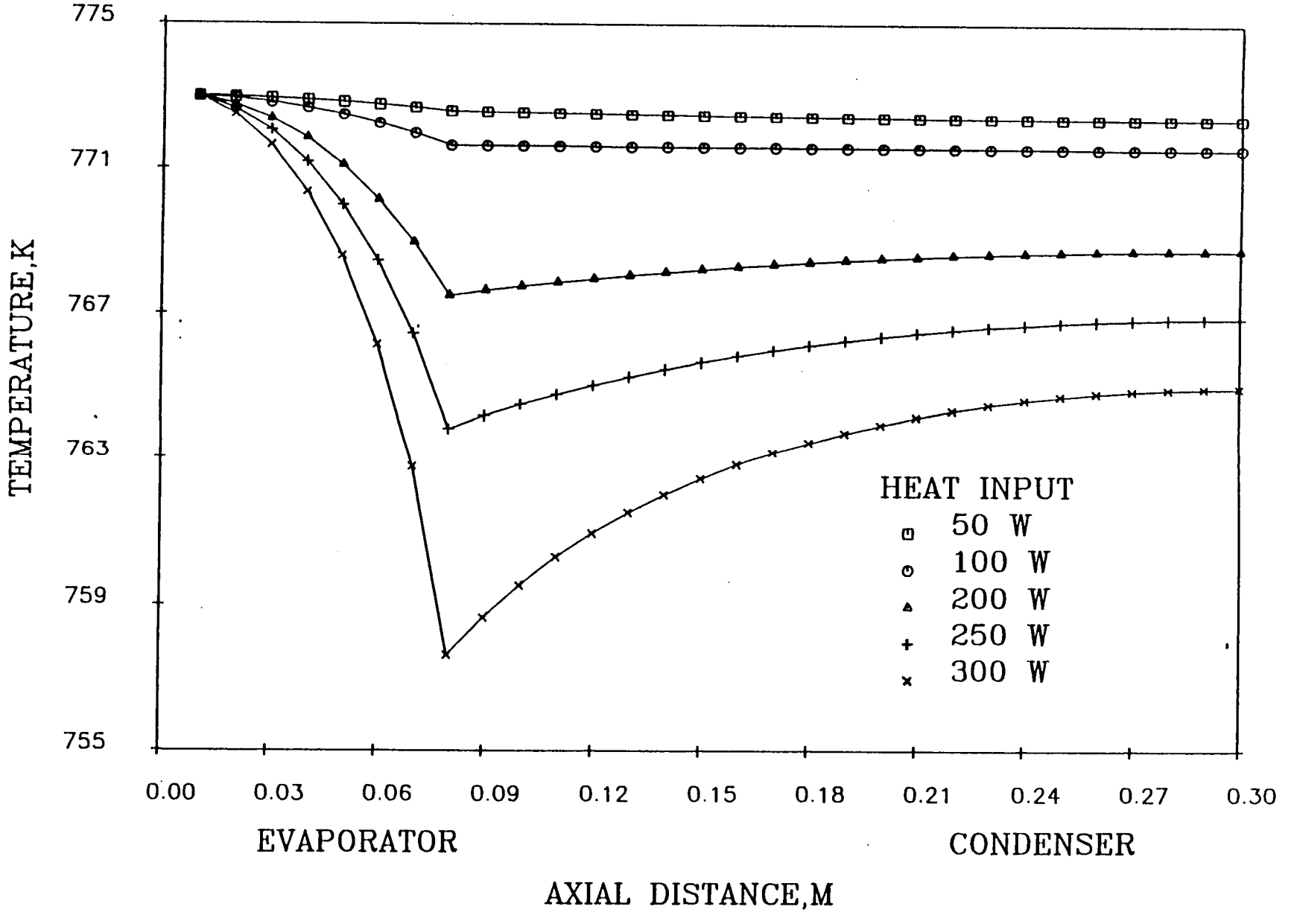

Figure 7. Axial variations of vapor temperatures for various heat inputs.

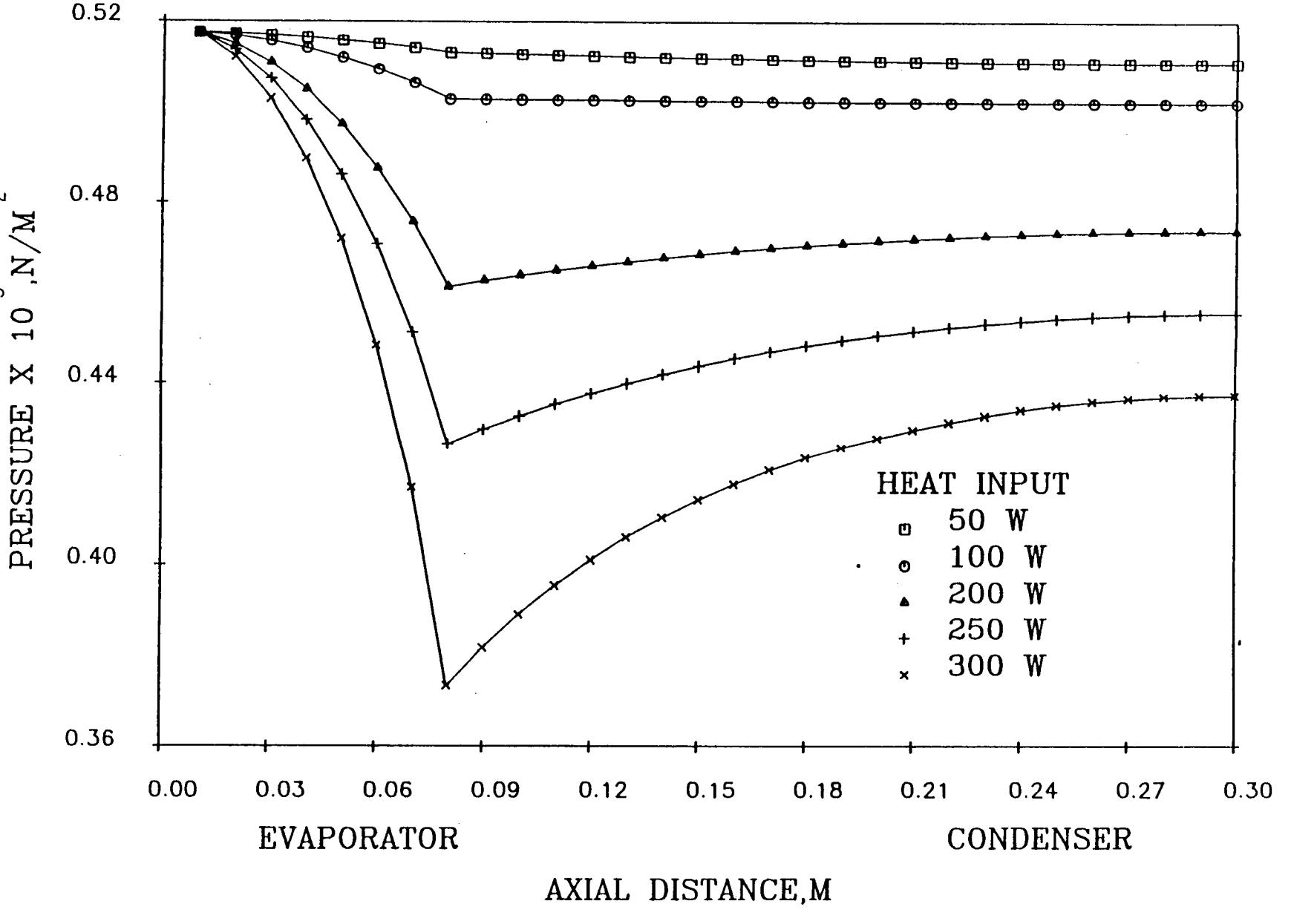

Figure 8. Axial variations of vapor pressures for various heat inputs.

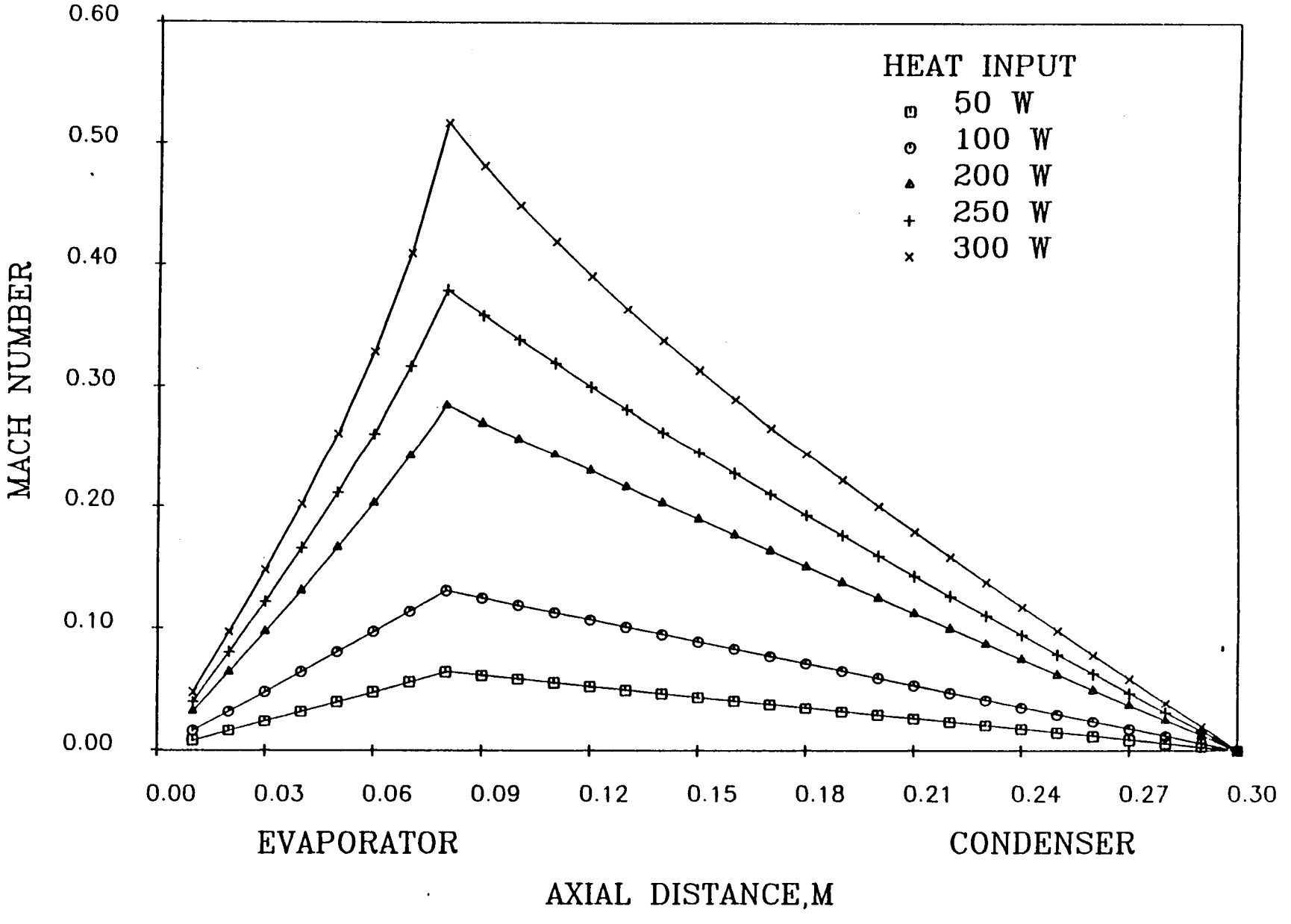

Figure 9. Axial variations of Mach numbers for various heat inputs.

the Mach number exceeds about .2, the variation of the Mach number is large due to expansion of the vapor. For heat inputs of 50 and 100 watts, the vapor can be assumed to be isothermal.

Figure 10 shows that the possible maximum heat transfer is limited to about 351 watts because the Mach number at the end of the evaporator approaches the sonic velocity.

Figure 11 presents axial variations of vapor temperature, pressure, velocity, and density at the operating temperature of 808 K. For this case, the operating temperature is 35 K higher, but pressure and density are twice as high than for 773 K. Thus, the velocity is small and the maximum Mach number is only about 0.2. This leads to a small pressure drop, and the corresponding temperature drop is about 2.8 K. Even though the heat input is twice as much as that for 773 K, a comparison of temperature drops implies that pressure and temperature drops mainly depend on the operating temperature.

In the adiabatic section, there is no mass injection or extraction. Hence, pressure simply decreases due to friction, and the velocity increases very little. The contribution of the adiabatic section is the addition of pressure and temperature drops such that for the high Mach number at the exit of the evaporator, the maximum heat transfer rate is reduced considerably. Figure 12 shows this phenomenon. The heat input of 865 watts results in a Mach number of 0.7 at the exit of the evaporator. Then, the vapor is accelerated in the adiabatic section, so the velocity of vapor approaches the sonic velocity at the end of this section.

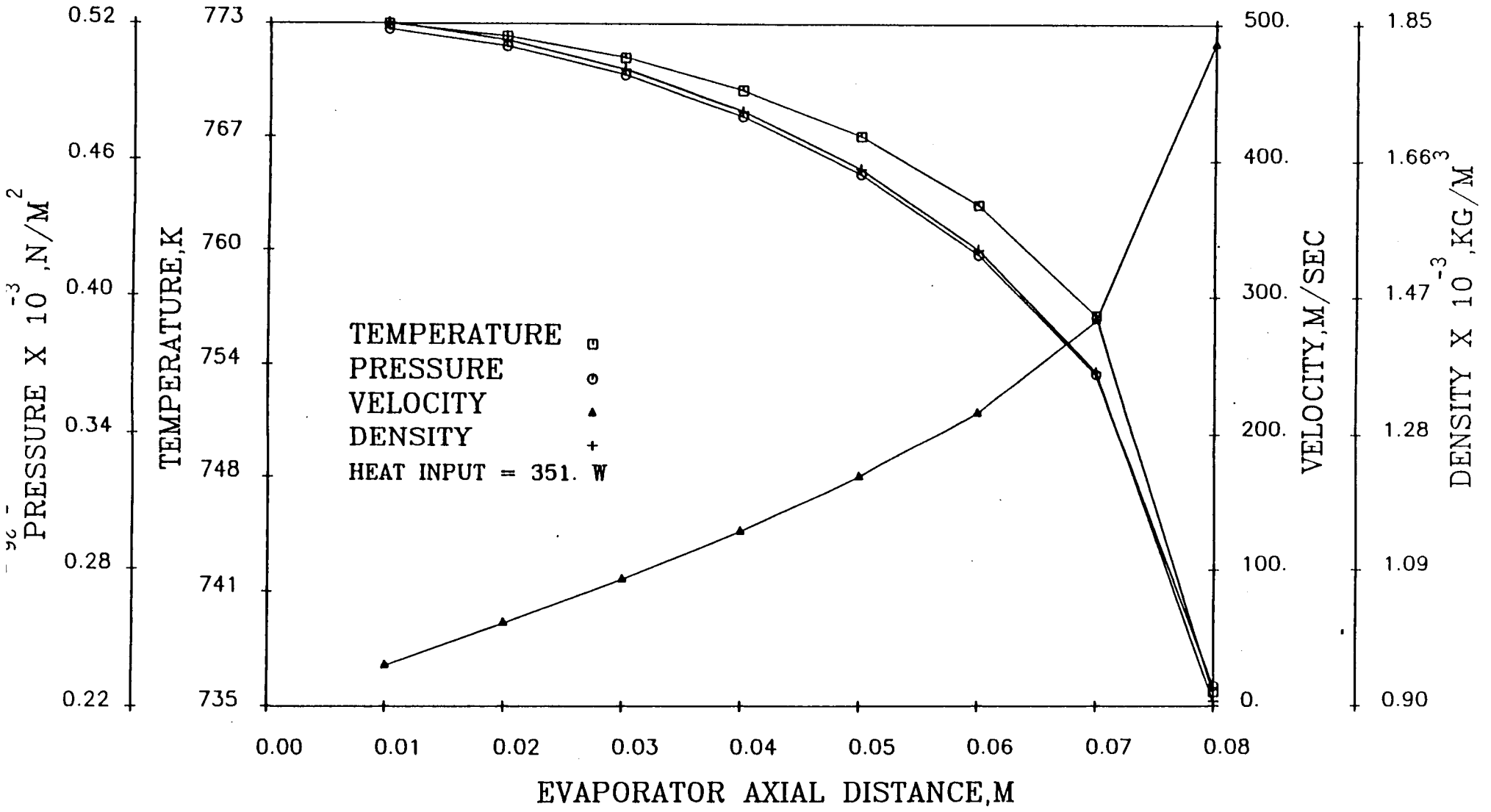

Figure 10. Axial variations of vapor temperature, pressure, velocity, and density at the sonic limit condition for operation temperature of 773 k.

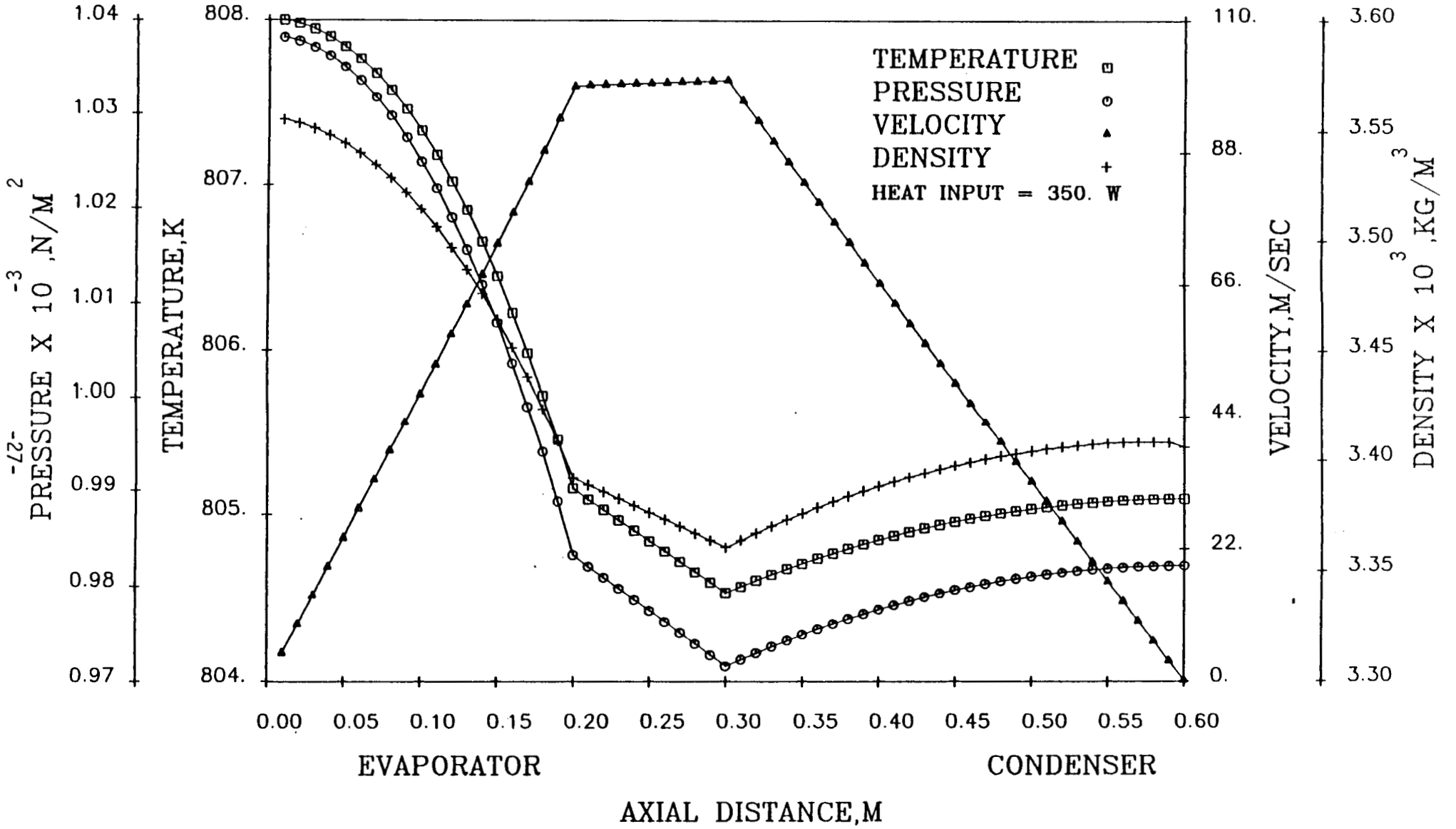

Figure 11. Axial variations of vapor temperature, pressure, velocity, and density at operating temperature of 808 k.

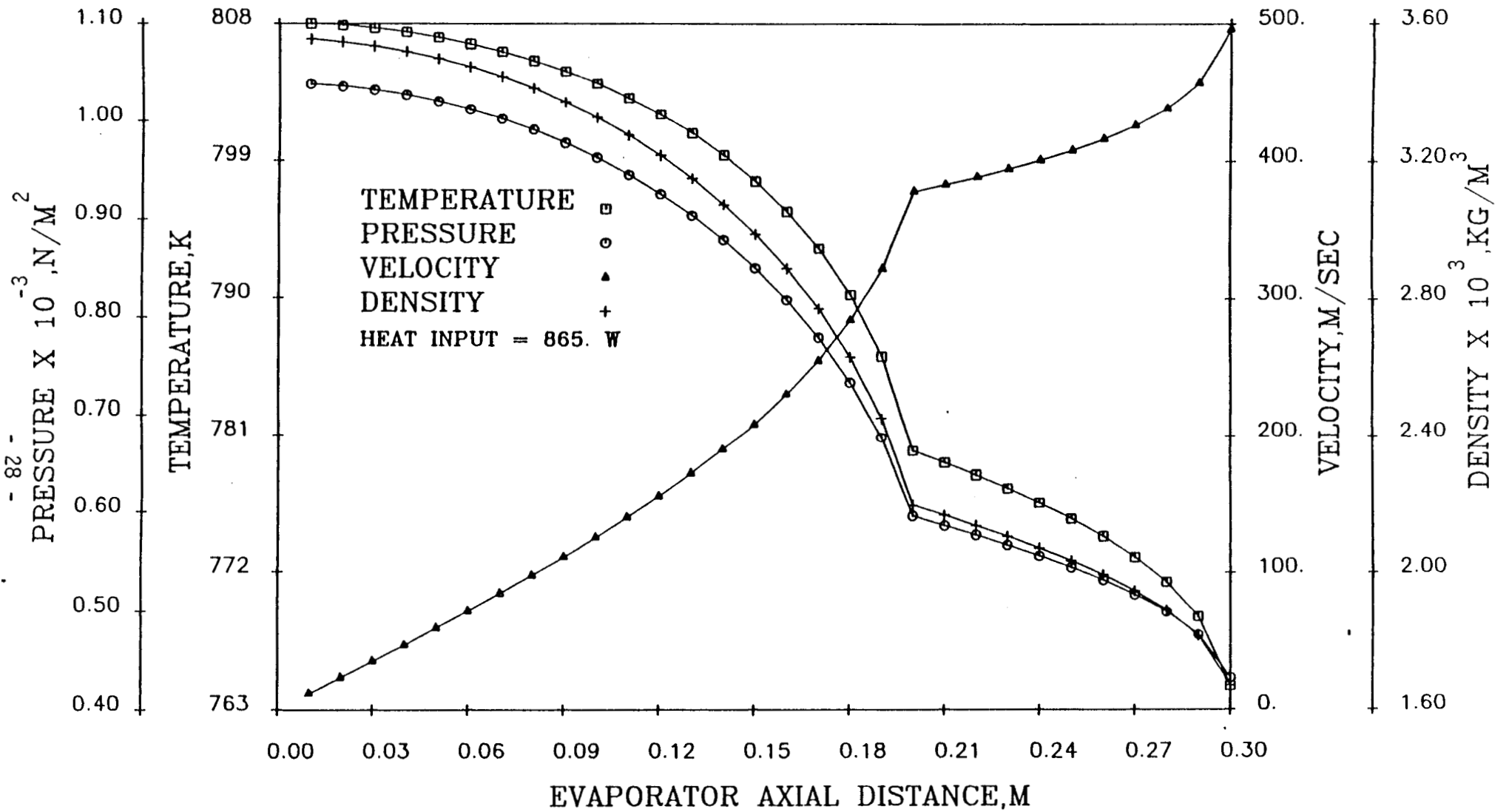

Figure 12. Axial variations of vapor temperature, pressure, velocity, and density at sonic limit condition for operating temperature of 808 k.

In the condenser section, as expected, the pressure and temperature drops are recovered, but the degree of recovery is small due to small vapor velocity and large friction loss in the longer condenser. Numerical results show that the temperature recovery is only 0.6 K.

Variations of temperature, pressure, and Mach number corresponding to six different heat fluxes at the operating temperature of 808 K are presented in Figures 13, 14, and 15, respectively. For heat input up to 200 watts, pressure recovery is not observed. This implies that the pressure drop due to friction in the condenser may exceed the value of the inertial contribution. However, the total pressure drops are small, so the vapor can be assumed to be isothermal.

Figure 16 shows the distributions of the nonuniform heat flux on the evaporator and condenser. Axial variations of vapor temperature, pressure, velocity, and density corresponding to the distribution in Figure 16.a are presented in Figure 17. At a short distance away from the beginning of the condenser, the slight heat extraction suggests that the axial variation of the vapor velocity is small. Thus, the friction effect in this region is dominant. The minimum temperature and pressure appear in the condenser instead of at the exit of the evaporator. As the heat extractions increase, the absolute value of axial variation of velocity increases and the vapor velocity decreases. The pressure drops are recovered gradually. In Figure 18, corresponding to the distribution in Figure 16.b, the temperature and pressure drops are recovered immediately from the beginning of the condenser due to the large heat extraction. As expected, axial variations of temperature, pressure, velocity, and density depend on the distributions of heat input.

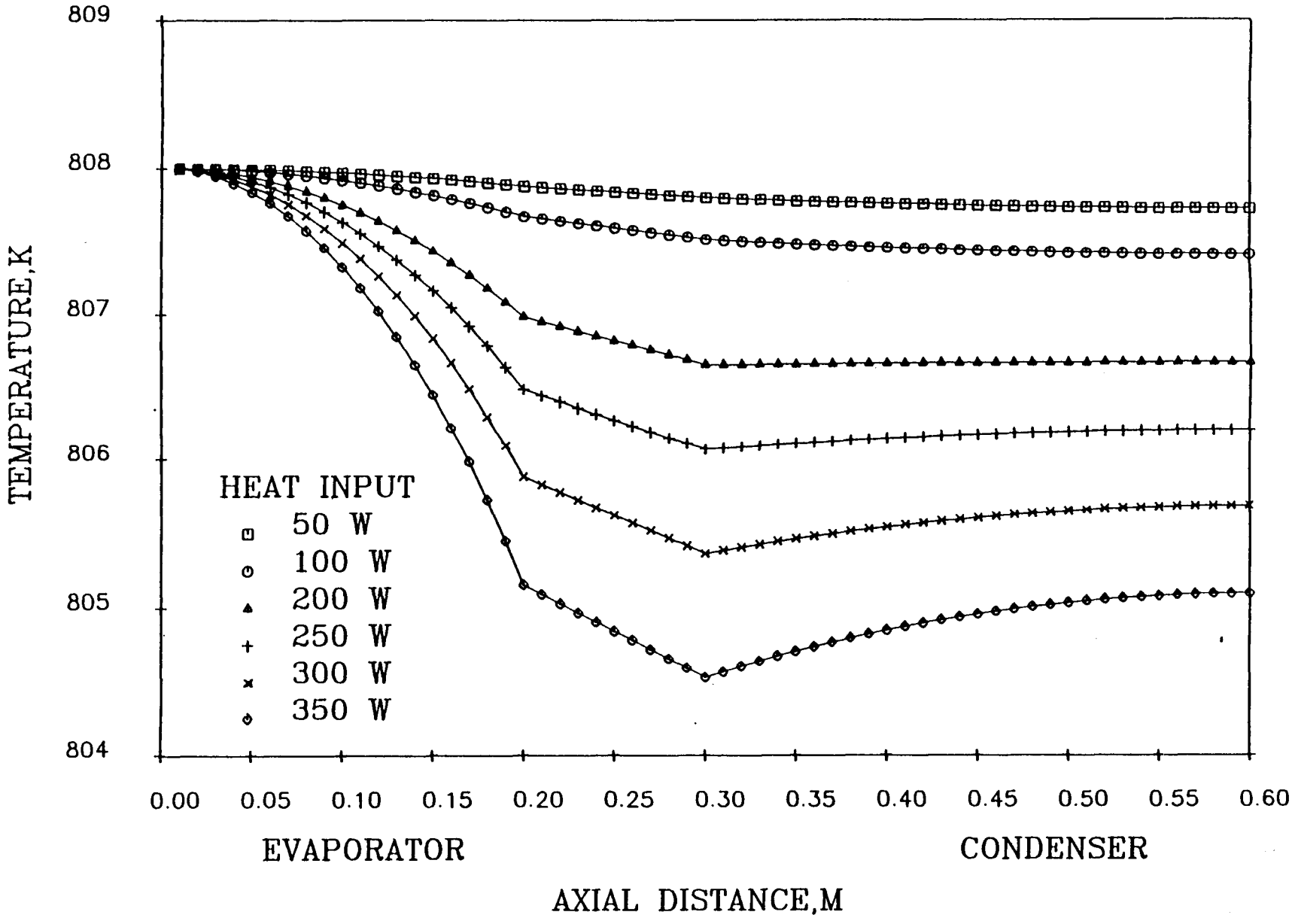

Figure 13. Axial variations of vapor temperatures for various heat inputs.

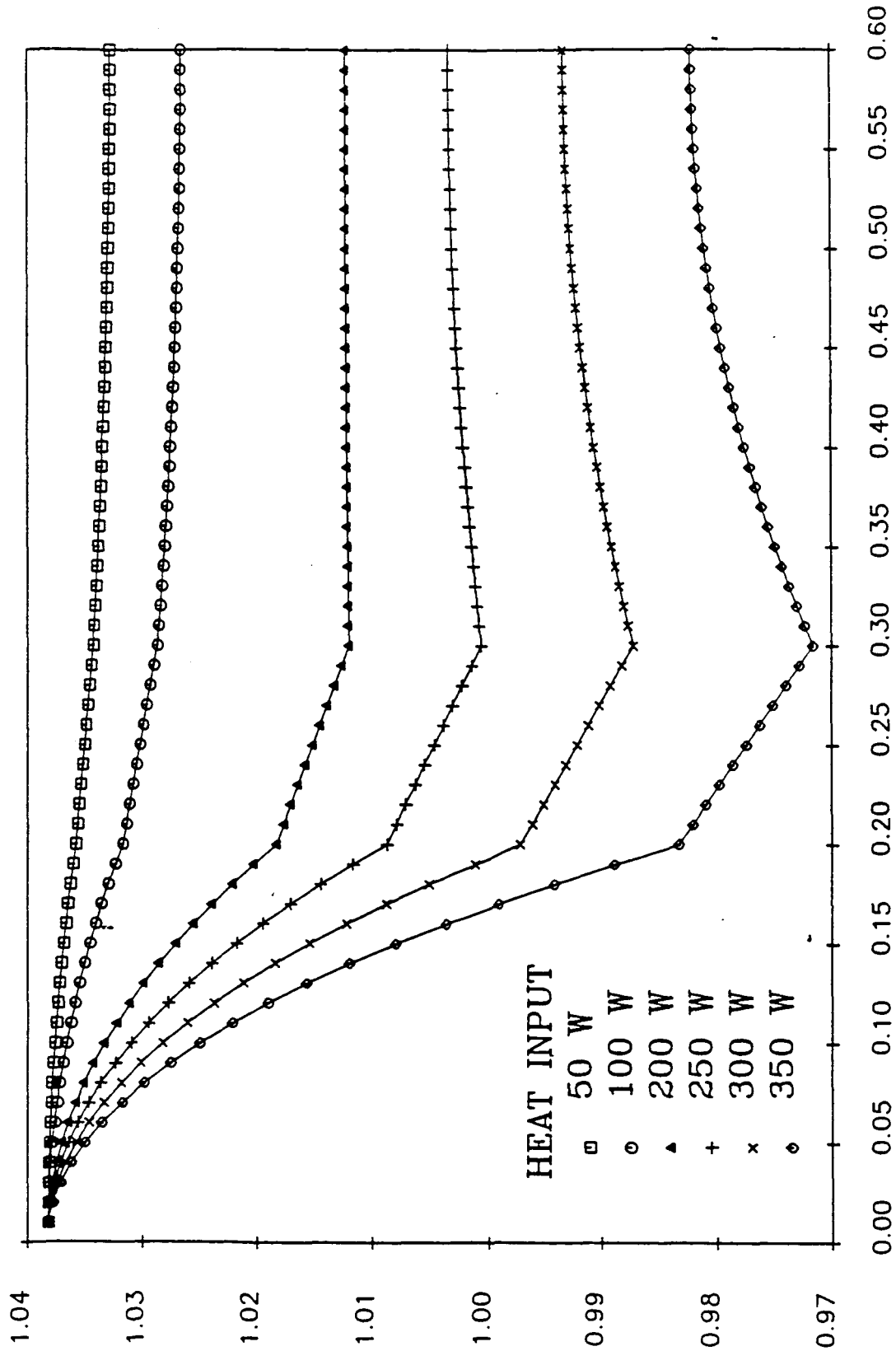

Figure 14. Axial variations of vapor pressure for various heat inputs.

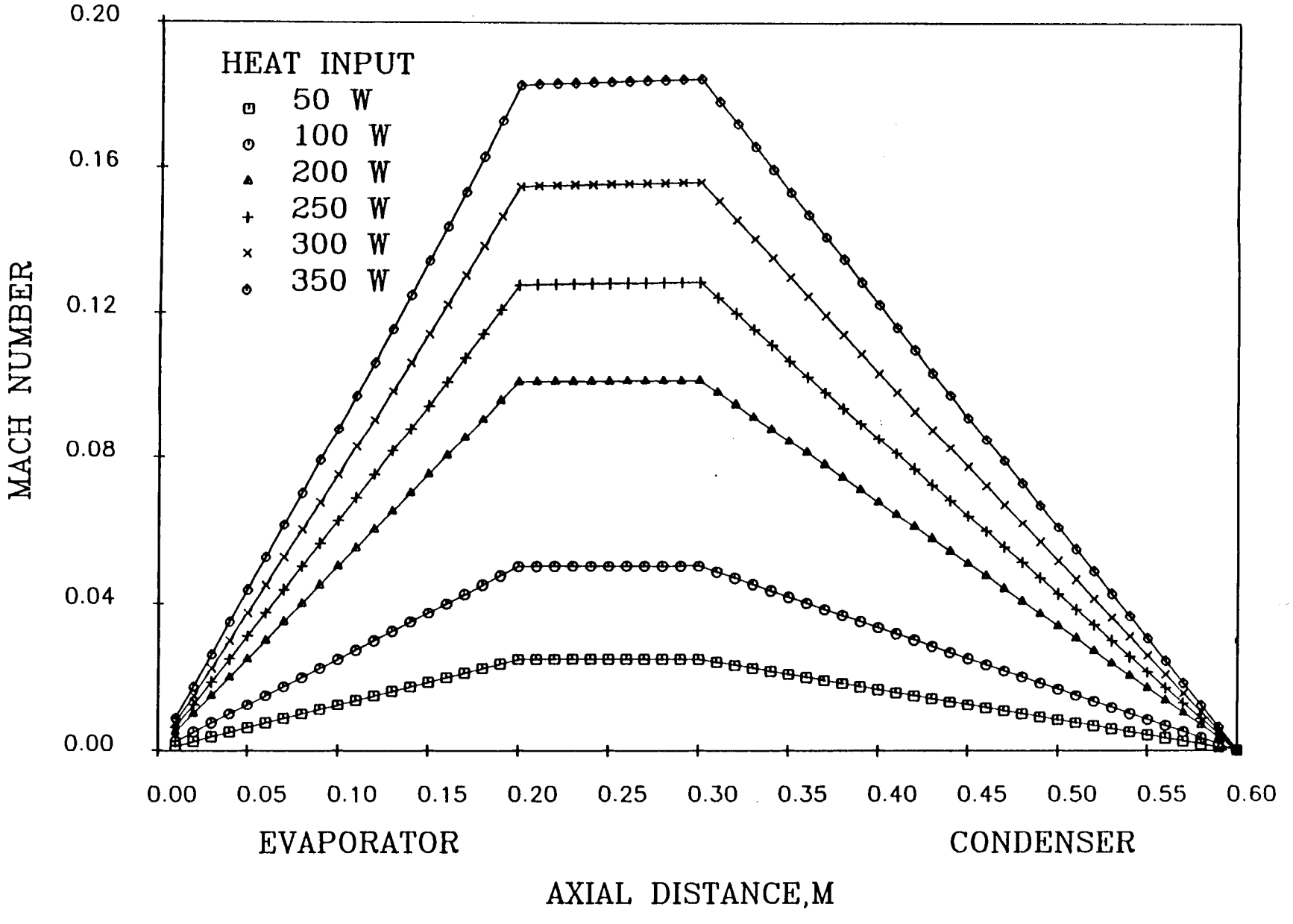

Figure 15. Axial variations of Mach numbers for various heat inputs.

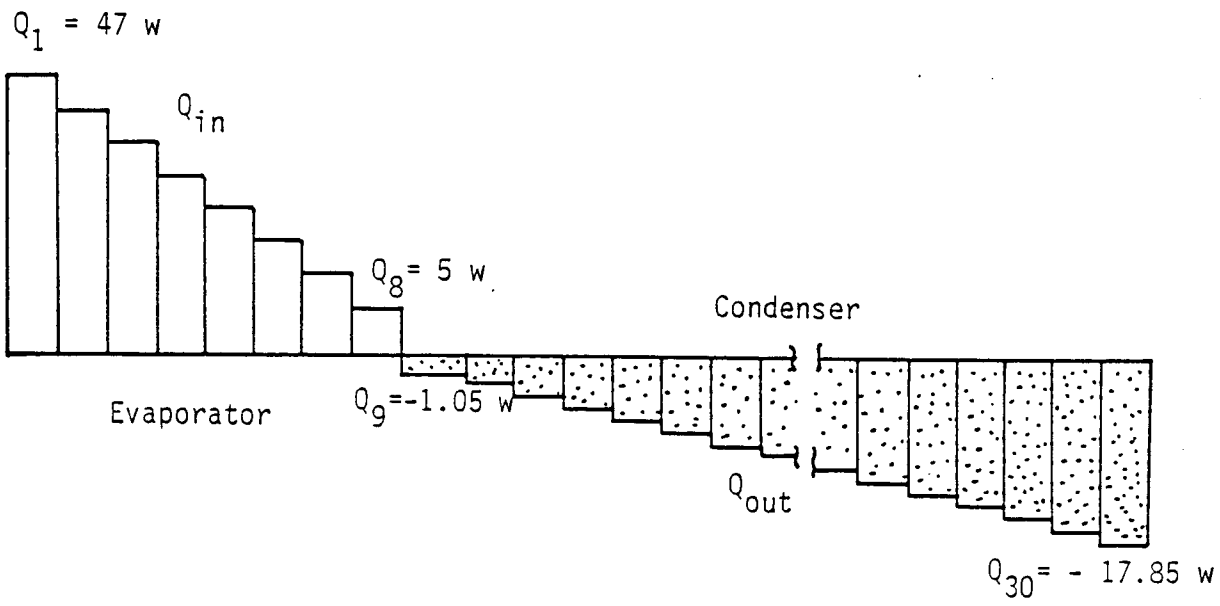

16.a)

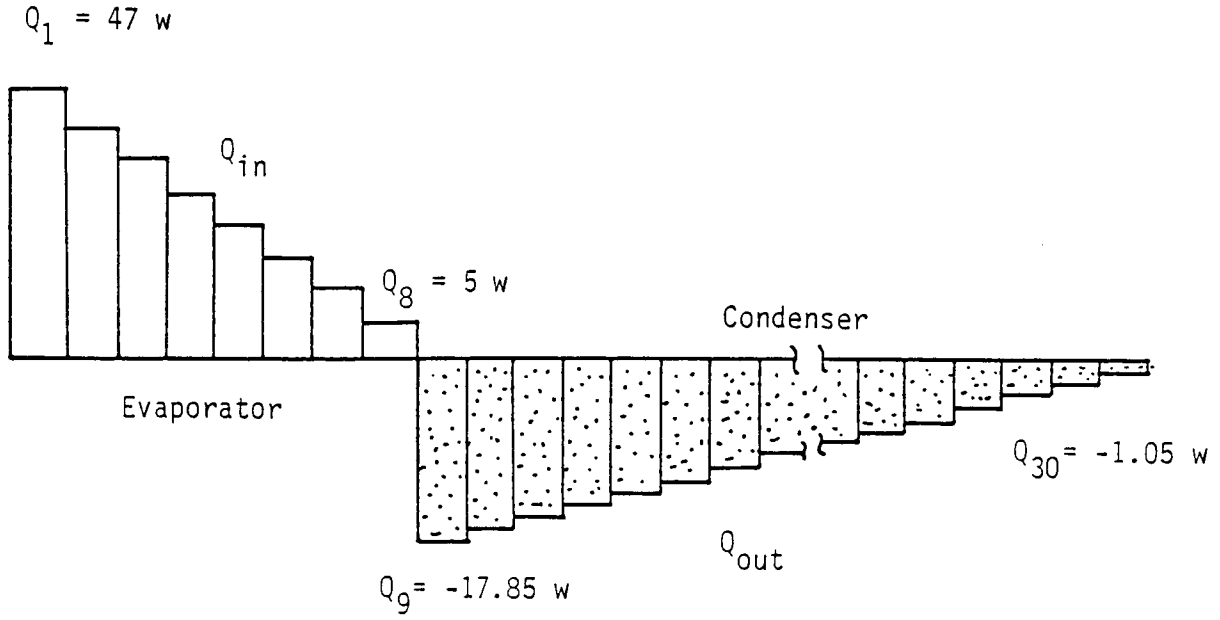

16.b)

Figure 16. Distribution of heat input on the evaporator and condenser.

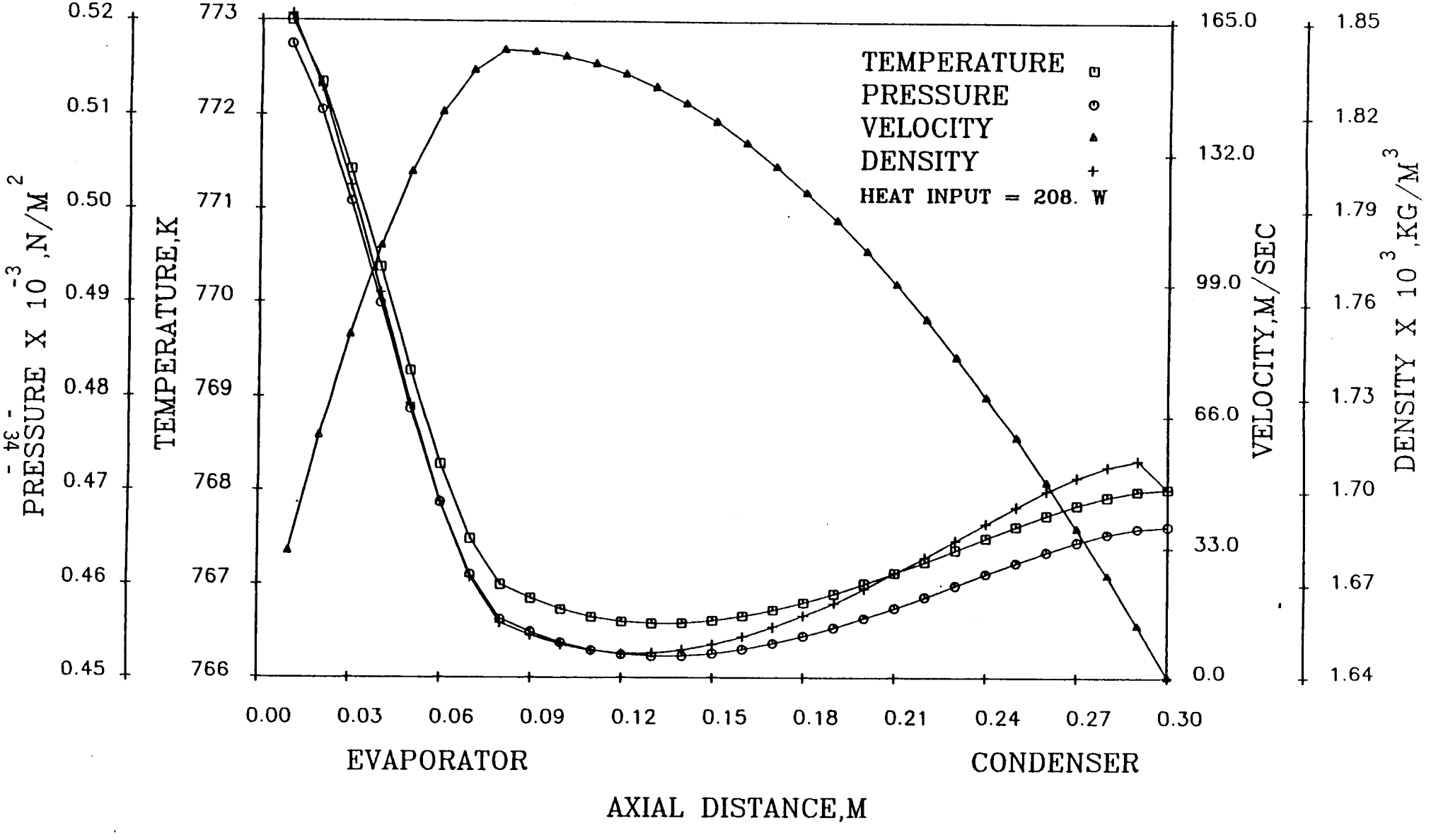

Figure 17. Axial variations of vapor temperature, pressure, velocity, and density for nonuniform heat input in figure 16a.

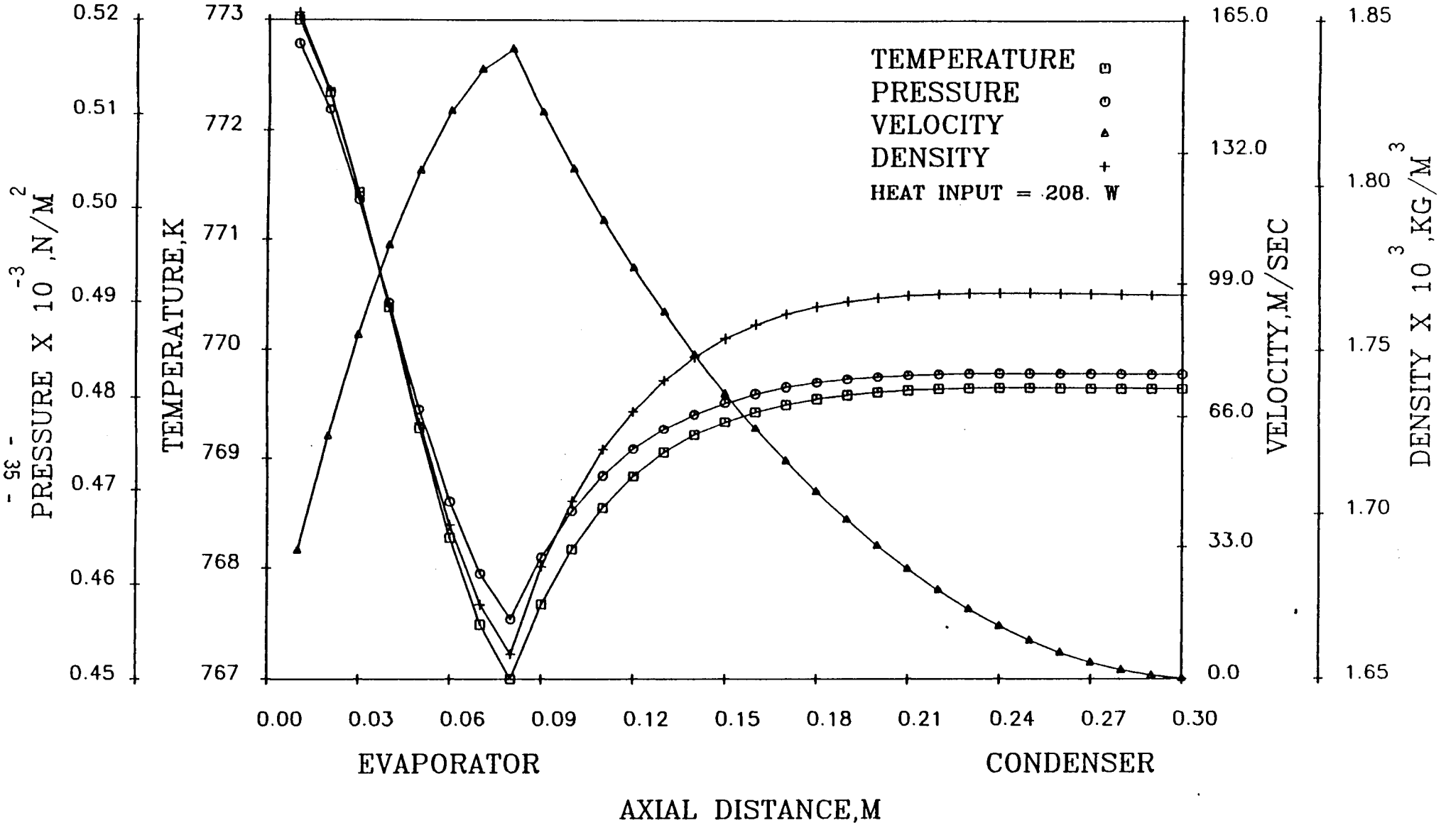

Figure 18. Axial variations of vapor temperature, pressure, velocity, and density for nonuniform heat input in figure 16b.

In summary of the results, the degree of pressure recovery mainly depends on the heat flux, operating temperature, and length of the condenser. The higher the heat flux, the lower the operating temperature, and the shorter the condenser, the greater the pressure recovery. However, for this case, the pressure drop in the evaporator can be large enough that the entire heat pipe is not isothermal.

Since experimental data is not available, quantitative comparison can not be achieved. However, comparison of the general behavior of the present results with published data[2,6,7] gives qualitative agreement.

REFERENCES

1. C. L. Tien, "Fluid Mechanic of Heat Pipes," Annual Review of Fluid Mechanics, Vol. 7, 1975, PP. 167-185.
2. M. N. Ivanovskii, V. P. Sorokin, and I. V. Yagodkin, "The Physical Principles of Heat Pipe", Clarender Press, Oxford, 1982.
3. P. L. Donoughe, "Analysis of Laminar Incompressible Flow in Semiporous Channels," NACA TN 3759, August, 1956.
4. E. R. G. Eckert, P. L. Donoughe, and B. J. Moore, "Velocity and Friction Characteristics of Laminar Viscous Boundary-Layer and Channel Flow over Surfaces with Ejection or Suction," NACA TN4102, December 1957.
5. C. A. Bankston and H. J. Smith, "Incompressible Laminar Vapor Flow in Cylindrical Heat Pipe," ASME Paper NO 71-WA/HT-15 , 1972.
6. E. K. Levy, "Theoretical Investigation of Heat Pipes Operating at Low Vapor Pressures," J. Engineering for Industry, Nov. 1968, PP. 547-552.
7. C. L. Tien and A. R. Rohani, "Analysis of the Effects of Vapor Pressure Drop on Heat Pipe Performance," Int. J. Heat Mass Trans, Vol. 17, PP. 1974, 61-67.

LIST OF SYMBOLS

A_o	area of porous wall of injection or suction section
C_{pf}	constant pressure specific heat of liquid
D	thickness of vapor passage
f	dimensionless stream function
F	friction factor
h	enthalpy of vapor
h_f	enthalpy of saturated liquid
h_{fg}	latent heat of vaporization
h_o	enthalpy of vapor at interface
L_e	length of evaporator
L_a	length of adiabatic section
L_c	length of condenser
$\dot{m}_o$	mass injection or suction rate per unit area
P	pressure
Q	quality of vapor
R	gas constant
Re_o	wall Reynolds number
T	temperature
u	z-component of velocity
U*(0)	average velocity at z = 0
v	specific volume of vapor
v_f	specific volume of saturated liquid

v_g	specific volume of saturated vapor
v^*_o	velocity at porous wall
v^*	y-component of velocity
V	average velocity at cross section
W	width of vapor passage
X	vapor quality
y	coordinate direction normal to axial direction
Z	coordinate in axial direction

Greek Symbol

α	momentum factor
β	energy factor
λ	dimensionless length coordinate
ν	kinetic viscosity
ρ	density of vapor
ρ_o	density of vapor at interface
τ_v	shear stress
ψ	stream function